journal of the mechanical behavior of biomedical materials 137 (2023) 105536

Contents lists available at ScienceDirect

Journal of the Mechanical Behavior of Biomedical Materials

journal homepage: www.elsevier.com/locate/jmbbm

An explorative study on the antimicrobial effects and mechanical properties of 3D printed PLA and TPU surfaces loaded with Ag and Cu against nosocomial and foodborne pathogens

Sotirios I. Ekonomou [a], Shwe Soe [b,1], Alexandros Ch. Stratakos [a,1,*]

[a] College of Health, Science and Society, School of Applied Sciences, University of the West of England, Coldharbour Ln, Bristol, BS16 1QY, UK
[b] College of Arts, Technology and Environment, School of Engineering, University of the West of England, Coldharbour Ln, Bristol, BS16 1QY, UK

ARTICLE INFO

Keywords:
3D printing
Polymers
Biofilm
Pathogens
Healthcare
Food sector

ABSTRACT

Antimicrobial 3D printed surfaces made of PLA and TPU polymers loaded with copper (Cu), and silver (Ag) nanoparticles (NPs) were developed via fused deposition modeling (FDM). The potential antimicrobial effect of the 3D printed surfaces against *Escherichia coli*, *Listeria monocytogenes*, *Salmonella* Typhimurium, and *Staphylococcus aureus* was evaluated. Furthermore, the mechanical characteristics, including surface topology and morphology, tensile test of specimens manufactured in three different orientations (XY, XZ, and ZX), water absorption capacity, and surface wettability were also assessed. The results showed that both Cu and Ag-loaded 3D printed surfaces displayed a higher inhibitory effect against *S. aureus* and *L. monocytogenes* biofilms compared to *S. Typhimurium* and *E. coli* biofilms. The results of SEM analysis revealed a low void fraction for the TPU and no voids for the PLA samples achieved through optimization and the small height (0.1 mm) of the printed layers. The best performing specimen in terms of its tensile was XY, followed by ZX and XZ orientation, while it indicated that Cu and Ag-loaded material had a slightly stiffer response than plain PLA. Additionally, Cu and Ag-loaded 3D printed surfaces revealed the highest hydrophobicity compared to the plain polymers making them excellent candidates for biomedical and food production settings to prevent initial bacterial colonization. The approach taken in the current study offers new insights for developing antimicrobial 3D printed surfaces and equipment to enable their application towards the inhibition of the most common nosocomial and foodborne pathogens and reduce the risk of cross-contamination and disease outbreaks.

1. Introduction

As early as 460 B.C., it was Hippocrates who had early recognized a strong connection between food consumption and human infectious diseases causing illness (Bintsis, 2017). *Escherichia coli*, *Listeria monocytogenes*, *Salmonella* Typhimurium, and *Staphylococcus aureus* are some of the most common pathogens in the food industry and are regularly implicated in foodborne outbreaks. Amongst others, *S. aureus* is an important pathogen often contaminating surfaces and causing healthcare-associated infections and recently identified that it is most commonly associated with biofilms formed on hospital surfaces (Ledwoch et al., 2018). These pathogens have been shown to survive on surfaces for prolonged periods by forming biofilms which lead to cross-contamination. Improper cleaning and disinfection, in combination with rich in moisture and nutrients surfaces, create favorable conditions for bacterial adhesion and biofilm development (Ban and Kang, 2016). Bacteria living in biofilm communities form an extracellular polymeric substance (EPS) matrix, which protects them against various disinfectants compared to their planktonic derivatives.

Numerous researchers have studied the effectiveness of sanitizers used in the food industry and healthcare sector against bacterial pathogens to clean and disinfect surfaces and prevent biofilm formation (Ban and Kang, 2016; Carpentier and Cerf, 2011; Lineback et al., 2018). However, the increased antimicrobial resistance has led to the search for new combinations of treatments with sanitizers and using new natural alternatives to improve the ability of biofilm inhibition and removal (Ashrafudoulla et al., 2021; Ban and Kang, 2016). Conventional approaches using chlorine-based sanitizers, heat, ultraviolet, and gamma

* Corresponding author.
E-mail address: alexandros.stratakos@uwe.ac.uk (A.Ch. Stratakos).
[1] Shwe Soe and Alexandros Ch. Stratakos jointly directed this work.

https://doi.org/10.1016/j.jmbbm.2022.105536
Received 23 September 2022; Received in revised form 16 October 2022; Accepted 19 October 2022
Available online 29 October 2022

irradiation have been extensively studied and sometimes proved expensive and/or inefficient, while the use of non-chlorine-based disinfectants is limited by their short action duration and environmental safety (Siedenbiedel and Tiller, 2012).

3D printing is an additive manufacturing (AM) technique for fabricating a wide range of structures and complex shapes. Various 3D printing methods, materials, and equipment have evolved over the years (Ngo et al., 2018). Fused deposition modeling (FDM) is one of the most promising AM techniques broadly used for designing and developing medical devices and has started finding new applications in the food industry (Deb and Jafferson, 2021). One of the main challenges for this technology to be adopted is attributed to the development of antimicrobial surfaces that can come in contact with food and humans to control bacterial colonization and the spread of disease (González-Henríquez et al., 2019). The use of polymers synthesized by naturally occurring materials for AM applications has been increasing in the last years. Polylactic acid (PLA) and thermoplastic polyurethanes (TPU) are among the main polymers used in 3D printing because of their excellent mechanical properties (Jašo et al., 2015). PLA and TPU polymers were our main focus as they are both recyclable, biodegradable, and highly biocompatible polymers that have been widely used in the production of medical devices and are safe for humans (Cao et al., 2006; Choonara et al., 2016; Jašo et al., 2015). Other printable polymers, ranging from acrylonitrile butadiene styrene (ABS), polyamide, polycaprolactone (PCL), polyether ether ketone (PEEK) etc. have been used to fabricate biomedical devices including 3D scaffolds for tissue-engineered implants (Hutmacher et al., 2001), 3D printed antimicrobial wound dressings (Muwaffak et al., 2017), implants, and prosthetic parts (ten Kate et al., 2017).In order to provide antimicrobial properties to 3D printed materials, various strategies have been employed. Antimicrobial polymers are currently being produced by the incorporation of antimicrobial agents (Mai et al., 2020) and the use of hot melt extrusion, where polymer pellets can be combined with numerous metal alloys, ions, or nanoparticles (NPs) of copper (Cu), graphene (C), titanium (Ti), and silver (Ag) that may have antimicrobial properties (Ahmed et al., 2021). This introduces new properties to the composites and possibilities for their future use towards the development of medical and food equipment and surfaces (Sandler et al., 2014). Nowadays, a still remaining fundamental problem in the application of polymeric materials for biomedical and food applications is linked to their contamination by numerous pathogens (Kenawy et al., 2007). Although there is enough information to design and develop new 3D printing composite materials, there is not enough literature to date on their antimicrobial spectrum and how they can inhibit biofilm formation of pathogenic bacteria commonly found in the healthcare sector (Hall et al., 2021; Vidakis et al., 2020) and even less in the food sector.

The aim of the current study was to fabricate 3D printed surfaces using commercially available PLA and TPU filaments loaded with Cu and Ag-NPs using an FDM 3D printer. The antimicrobial properties and surface transferability of the 3D printed surfaces were investigated in depth against relevant nosocomial and foodborne pathogens. The mechanical properties and microstructural characteristics of the 3D printed surfaces were also investigated to ensure that the antimicrobial-loaded 3D printed surfaces offer a comparable performance to the plain counterparts.

2. Materials and methods

2.1. Materials studied

Filaments of plain PLA and TPU were purchased from KIMYA SAS (Nantes, France). The filaments with Cu and Ag blended additives were obtained from Copper3D (The Netherlands) and 3DFILAMENTS S.L. (Elche, Spain). The properties of the filaments used in the current study are presented in Table 1. All filaments purchased are odorless and compliant with European Union standards: No. 10/2011 for plastic materials intended to come into contact with food.

Table 1
Filament names and descriptions.

Filament	Diameter (mm)	Density (g/cm^3)	Printing speed (mm/s)	Infill (% w/w)	Filler morphology
PLA – HI	1.75 ± 0.1	1.21	40–150	–	–
TPU – 92A	1.75 ± 0.1	1.16	20–70	–	–
Copper3D PLACTIVE – PLA 850	1.75 ± 0.05	1.24	40–50	≤2.00	Cu oxide-NPs
Copper3D MD Flex – TPU98A	1.75 ± 0.05	1.16	20–75	≤2.00	Cu oxide-NPs
abFil – PLA 850	1.75 ± 0.02	1.24	20–65	≤2.00	Ag-NPs
abFil – TPU 90A	1.75 ± 0.01	1.19	20–40	≤2.00	Ag-NPs

2.2. Fabrication of 3D printed surfaces

All the filaments named PLA (plain), TPU (plain), PLA-Cu, TPU-Cu, PLA-Ag, and TPU-Ag were used to fabricate the 3D printed surfaces of 30 x 10 x 1 mm^3. The 3D printed surfaces were fabricated using an FDM 3D printer, Creator Pro 2 (Flashforge 3D Technology Co., Ltd, Zhejiang, China), with a full closed print chamber, independent dual extruder system, and a maximum build volume of 280 x 250 x 300 mm^3. In the fabrication process, the filaments were fed into a 0.4 mm diameter nozzle by a feeding pressure mechanism via a driver motor. The melted filament pushed through the nozzle was deposited on a pre-heated bed at 40^{o}C. The flashprint software was used to determine the slicing sequence and define the FDM process. All 3D printed surfaces were fabricated with an infill density of 100%, the first layer height of 0.20 mm, and the nozzle fan always on. The detailed fabrication parameters are presented in Table 2.

2.3. Characterization techniques of 3D printed surfaces

2.3.1. SEM analysis

The microscopic analysis of the layers' microstructure and surface morphology of the 3D printed surfaces fabricated with plain, Cu and Ag-loaded PLA and TPU was performed using the FEI Quanta 650 (Thermo fisher scientific, UK) field emission scanning electron microscope (SEM). The microscopic observation of the 3D printed surfaces required a thin layer of gold coating (~10 nm) that was deposited on their surface, using sputter coater Emscope SC500 (Quorum Technologies Ltd, Essex, UK), to make it conductive before the observation in SEM. Then, the samples were observed under a high vacuum with a voltage of 5 kV and 2 spots using the Everhart-Thornley detector (ETD) to form an image from secondary electrons from a depth of tens of nanometers. To observe

Table 2
Fabrication parameters of the 3D printed surfaces.

Parameters	Filament Type					
	PLA	TPU	PLA-Cu	TPU-Cu	PLA-Ag	TPU-Ag
Nozzle temperature (^{o}C)	210	220	200	220	210	210
Layer height (mm)	0.10	0.10	0.10	0.10	0.10	0.10
Base print speed (mm/s)	50	50	50	50	60	50
Travel speed (mm/s)	70	70	70	70	70	70
Extraction speed (mm/s)	35	30	35	35	35	50
Retraction speed (mm/s)	35	30	35	35	35	35

the internal morphology, the printed samples were carefully cut with a scalpel followed by a sputter gold coating and used for SEM imaging.

2.3.2. Wettability of the 3D printed surfaces

The surface wettability of the 3D printed surfaces was performed using the Optical Tensiometer (Attension theta lite, Biolin Scientific AB, Sweden) contact angle analyzer system. The wettability of 3D printed surfaces was employed with the sessile drop method at room temperature (25°C). All samples prior to the contact angle measurements were kept for drying at 50°C overnight. A microsyringe was employed to dispense a 5 μL droplet of deionized water on the surface of the 3D printed surfaces, while the droplet profile was recorded with a CCD video camera after 2 s. The reported values for each surface are representative of three droplets at three different locations.

2.3.3. Mechanical testing

Following BS ISO 527–1:2012 (ISO-International Organization for Standardization, 2012) and BS ISO 37:2011 guidelines (BS ISO 37, 2011) tensile specimens were created for hard plastic (PLA) and soft elastomer (TPU), respectively (Fig. 1A). The test specimens were then manufactured in three different orientations (XY, XZ and ZX) with respect to the build platform (Fig. 1B) following the generic principle given in BS EN ISO/ASTM 52921 (Technical Committee AMT/8, 2017). Using Instron Universal Testing Machine, the fabricated tensile specimens were subjected to the quasi-static loading rates of 1 mm/min for PLA and 100 mm/min for TPU, respectively. The specimens were tested to failure, and the extracted force and displacement values were converted into stress and strain curves.

2.3.4. Water absorption capacity

The water absorption capacity of the 3D printed surfaces was determined according to the standard test method for plastics, ASTM D570-98 (ASTM D, 2010). All 3D printed surfaces were first dried in an oven at 50°C, overnight and immediately immersed in distilled water for 24 h, at room temperature. After the immersion time, all samples were removed and weighed using an analytical digital balance that was accurate to the nearest 10^{-4} g. The final water absorption capacity (W_a) was calculated using Eq. (1).

$$W_a\,(\%) = \frac{W_i - W_d}{W_d} \times 100 \quad (1)$$

where W_i is the weight after immersion and W_d is the dry weight of the 3D printed surfaces.

2.4. Microbiological analysis

2.4.1. Bacterial strains and growth conditions

S. aureus (NCTC 12981) and *L. monocytogenes* (NCTC 11994) were chosen as Gram-positive, while *E. coli* (ATCC 25922) and *Salmonella enterica* serovar Typhimurium (*S.* Typhimurium, ATCC 14028) were chosen as Gram-negative species associated with medical and foodborne pathogens. All bacteria were used from a frozen stock stored at −80 °C in Cryoinstant vials with porous beads (Microbank, Pro-Lab Diagnostics, UK). A single bead from each stock culture was transferred aseptically in 10 mL of Mueller Hinton broth (MHB; Oxoid, UK) and incubated overnight at 37 °C. Then, from the overnight cultures, a 10 μL inoculum was transferred in 10 mL MHB and incubated at 37 °C for 24 h. To prepare the working cultures, the cells were centrifuged at 6500g for 10 min, washed twice and resuspended in 10 mL phosphate-buffered saline (pH 7.4; PBS; Oxoid, UK) to reach a final population of 10^{8-9} log CFU/mL.

2.4.2. Biofilm formation on 3D printed surfaces

To investigate the antimicrobial effect of the 3D printed surfaces, before use, all surfaces were methodically cleaned in pure ethanol and dried under sterile conditions. Then, the sterile 3D printed surfaces of 30 x 10 x 1 mm^3 were transferred into falcon tubes containing 6 mL of sterile saline water (0.85%, w/v) NaCl solution and an inoculum of 100 μL of each pathogen (separately) to yield inocula of approximately 10^{7-8} CFU/mL. The tubes were left for 2 h, at room temperature, without shaking, to allow planktonic cells' adhesion on the 3D printed surfaces. Following the initial adhesion, each 3D printed surface was rinsed on both sides with 3 mL of 0.85% (w/v) NaCl to remove the loosely or non-attached cells. Then each 3D printed surface was transferred into a new sterile falcon tube containing 6 mL Tryptic Soy broth (TSB, Oxoid, UK) and left to incubate at room temperature for 72 h, to simulate the environmental conditions (i.e., food processing plants, hospitals). Finally, after 48h, the 3D printed surfaces were removed and gently rinsed with saline water 0.85% (w/v) NaCl as described earlier and were transferred into new falcon tubes with fresh TSB.

The 3D printed surfaces of neat PLA and TPU were used as controls for the PLA, and TPU surfaces loaded with metal alloys of Cu and Ag.

2.4.3. Bacterial enumeration

For the bacterial enumeration of the adhered biofilm cells with different maturity, on the first day (0 h) and every 24 h intervals, the 3D printed surfaces were removed aseptically and added individually in a sterile falcon tube containing 6 mL MRD and 1 g glass beads caliber 0.1 mm diameter. The 3D printed surfaces were vortexed for 1 min to detach the biofilm cells. Subsequently, an aliquot of 1 mL of the detached cells was transferred in 9 mL MRD to prepare the appropriate 10-fold serial dilutions. Then, an aliquot of 100 μL was used from the appropriate 10-fold serial dilution and was spread plated on TSA. Finally, the plates were left to incubate at 37°C for 24 h, and the biofilm cells were expressed as Log CFU/cm^2.

2.4.4. Surface transferability test

All 3D printed surfaces with adhered biofilm cells of different maturity (0, 24, and 72h) were tested to investigate if they could prevent direct bacterial transfer. The test simulates the subsequent transfers of biofilm cells from the 3D printed surfaces to the environment after contact. Following the formation of biofilm cells of different maturity on the surface of the 3D printed surfaces as described earlier, the surfaces dried for 30 min under a laminar flow at room temperature and were pressed 36 consecutive times with 100 g pressure on the surface of Dey-Engley (DE) neutralizing agar (Merck KGaA, Darmstadt, Germany). Then, DE agar was allowed to incubate overnight at 37 °C. Positive growth was indicated by a color change from purple to yellow. The transferability was expressed as the number of positive contacts divided by the total number of compressions, according to Ledwoch et al.

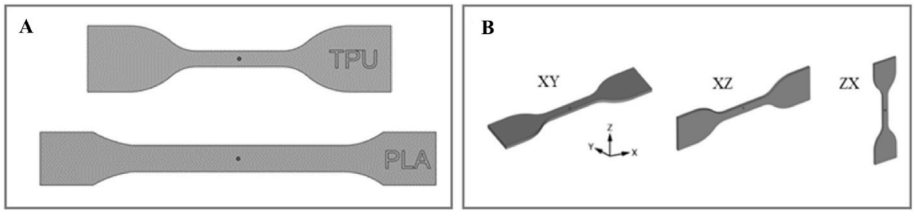

Fig. 1. Tensile specimen configurations (A) and manufactured orientations (B).

(2019).

2.5. Statistical analysis

All experiments were performed on three separate occasions. All data were expressed as mean ± standard deviation (SD) using Excel Microsoft® Office 365 (ver. 16.48). All data were subjected to a one-way analysis of variance by ANOVA test using the IBM® SPSS® statistics 26 software for macOS (SPSS Inc.). For data that showed a normal distribution, Student's t-test was used to determine significance at a level of 5%.

3. Results and discussion

3.1. SEM and microstructural analysis of the 3D printed surfaces

The microstructural analysis of the flat and fractured (cross-section) surface of the 3D printed samples was performed using SEM. The micrographs of the flat surfaces are presented in Figs. 2–4, and the cross-sections in Figs. 5–7. At low magnification, the fabrication quality of the 3D printed samples using the different filaments was demonstrated by investigating the interfacial defects, bilayer adhesion, and morphologies. At higher magnifications, the presence of Cu and Ag-NPs was exposed.

In Fig. 2A and B it can be seen clearly that the deposition of molten PLA and TPU, respectively, was satisfactory with good bilayer adhesion without inducing a fabrication failure. A smooth surface was observed for the 3D printed samples with PLA-Cu (Fig. 3A), while a wrinkled interlayer adhesion can be seen for the surfaces printed using TPU-Cu filament (Fig. 3B). The presence of the Cu particles became evident on the surface of the flat surfaces of both PLA-Cu and TPU-Cu samples. The size of the filler Cu-NPs ranged from 50 to 250 nm, as can be seen in Fig. 3A and B. The observation of spherical Cu-NPs on the surface of the commercial filaments loaded with Cu, in agreement with the current study, has been reported previously (Alam et al., 2020). SEM images of both PLA-Ag and TPU-Ag showed similar results, revealing a smooth surface and excellent interlayer adhesion. The Ag-NPs were more evenly spread on the surface of the TPU-Ag sample, while their shape was spherical primarily and, in some cases, had more pointy edges. The synthesis of stable, monodisperse, shaped Ag-NPs has been complex, partially because of the physio-chemical or biological methods used for their synthesis. In particular, Ag-NPs can be formed into various shapes, including rod, spherical, triangle, polyhedral, nanowires etc. (Lee and Jun 2019). Alam et al. (2020) verified the presence of flake-shaped Ag-NPs in commercial PLA-Ag 3D printed samples, while Podstawczyk et al. (2020) observed the synthesis of spherical Ag-NPs (50–200 nm) after producing their antimicrobial PLA filament loaded with Ag. In general, for all samples, it was observed that Ag and Cu-NPs are not only embedded in the polymer matrix but also cover its surface, which will come in direct contact with the external environment and tackle the growth and biofilm formation of the bacterial pathogens.

Observing the cross-sections for plain PLA (Fig. 5A) revealed the high quality of bonding of the layers without any voids. On the other hand, the cross-sectional SEM images at low magnification for the plain TPU (Fig. 5B) revealed the presence of voids in the middle of the sample. The same feature was also observed for the TPU-Cu and TPU-Ag samples. The apparent interlayer void observed in the mesostructure of the TPU samples ranged from 1 to 3 μm and is well known to take place when printing surfaces using flexible material. This drawback can be further optimized by lower printing speed at higher temperatures to improve the interaction and inter-joining between mesostructure interlayers determining a higher quality of bonding (Aliheidari et al., 2017). The homogeneous dispersion of Cu-NPs in the PLA-Cu matrix is one of the most important criteria and was evident at higher magnification in Fig. 6A. The SEM cross-sectional images of the PLA-Ag (Fig. 7A) and TPU-Ag (Fig. 7B) further confirmed the presence and the shape of the Ag-NPs in the 3D printed samples. Closely examining some large particles revealed subtle cluster features of both Cu and Ag-NPs.

Overall, it is interesting to mention that the 3D printing process led to a meager void fraction for the TPU and no voids for the PLA samples with or without metal alloys. It is well known that FDM printing tends to produce large gaps or voids between deposited layers. However, in compliance with the observations of Arif et al. (2018), low or no void fraction was achieved through optimization and choosing a 100% infill density, a small layer height (0.1 mm), and a higher nozzle temperature of 200–210°C for PLA and 220°C for TPU that increased the polymer's flow. The high initial quality of 3D printing is the first vital step to manufacturing food and biomedical equipment and surfaces with high mechanical performance and excellent antimicrobial properties. Utilizing X-ray photoelectron spectroscopy (XPS), in addition to SEM analysis would have offered extra information regarding the presence of Cu and Ag on the material surface.

3.2. Surface wettability of 3D printed surfaces

Surface wettability test was carried out to evaluate the influence of Cu and Ag content on the 3D printed surfaces. The results presented in Fig. 8 revealed that the surfaces printed with plain PLA had an average contact angle of 49.3 ± 2.49° compared with the 44.6 ± 11.92° for the plain TPU. Meanwhile, the 3D printed surfaces with Cu or Ag addition revealed a higher contact angle for both PLA and TPU material, meaning lower surface wettability. The decrease in the surface wettability could be attributed to the presence of Cu or Ag-NPs. Cu-loaded 3D printed surfaces presented the highest contact angle with 54.3 ± 3.79° and 84.3 ± 9.28° compared with 54.0 ± 9.53° and 64.8 ± 6.95° for the Ag-loaded 3D printed surfaces, respectively. Our results are in accordance with the

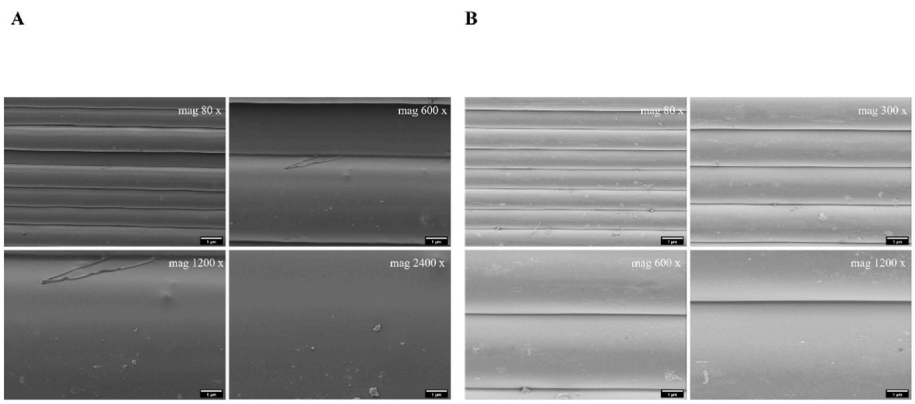

Fig. 2. Scanning electron microscope (SEM) images of plain (A) PLA and (B) TPU filament flat surface with increasing magnification.

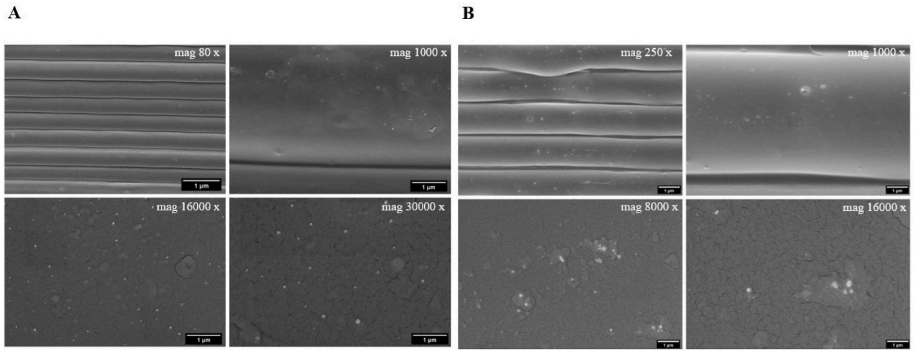

Fig. 3. Scanning electron microscope (SEM) images of (A) PLA-Cu and (B) TPU-Cu filament flat surface with increasing magnification.

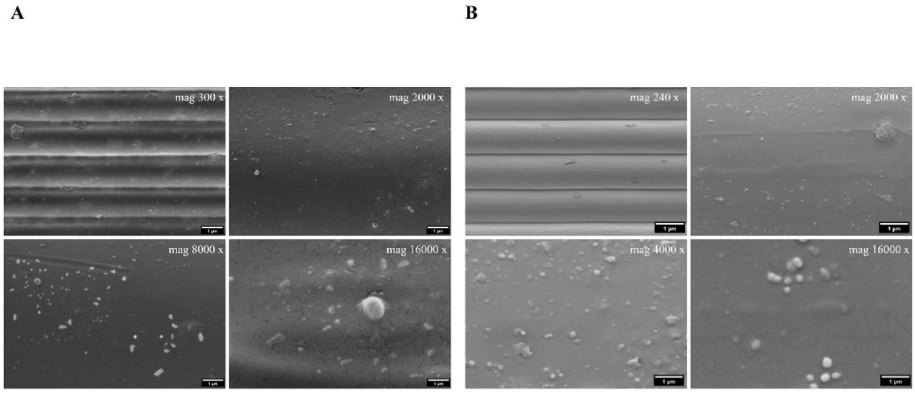

Fig. 4. Scanning electron microscope (SEM) images of (A) PLA-Ag and (B) TPU-Ag filament flat surface with increasing magnification.

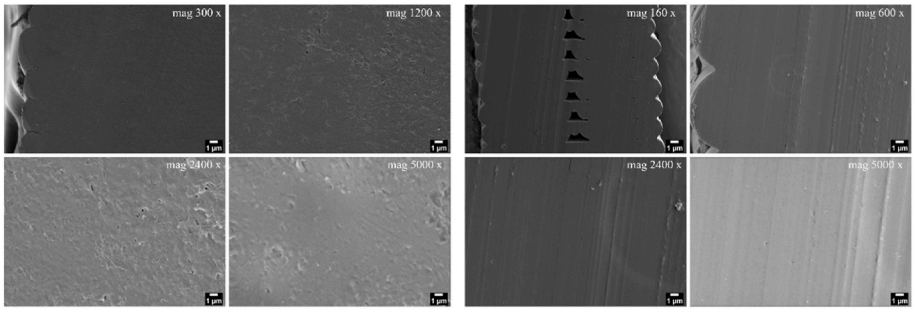

Fig. 5. Scanning electron microscope (SEM) images of plain (A) PLA and (B) TPU filament cross-section with increasing magnification.

study of Alam et al. (2020), where they observed a decrease in surface wettability of their 3D printed scaffolds using filaments loaded with bronze and Cu-NPs, while no significant change in the wettability was observed for the scaffolds printed using Ag loaded filament. On the other hand, Vidakis et al. (2020) reported that PLA-Ag 3D printed surfaces with a printing layer thickness same as the one used in the current study of 0.1 mm exhibited a high H_2O contact angle leading to antiadhesive surfaces that can be easily cleaned. Interestingly, by decreasing the printing layer height, the surface roughness is also decreased, leading to nanostructured surfaces with higher hydrophobicity that can be used in biomedical and food applications preventing the initial bacterial colonization and the subsequent formation of biofilms.

3.3. *Water absorption capacity of 3D printed surfaces*

Following the investigation of the 3D printed surfaces' wettability, it was crucial to examine their water absorption capacity. Water absorption represents a fundamental challenge for different composites as it can affect the mechanical performance and the properties of the composites (Quino et al., 2020). Fig. 9 shows the water absorption capacity of the different 3D printed surfaces used in this study.

The standard test method for plastics, ASTM D570-98, was used to determine the amount of distilled water absorbed from the different 3D printed surfaces after their immersion for 24 h. All the surfaces printed with PLA with or without metal alloy addition revealed the lowest water absorption capacity without statistically significant differences (Fig. 9; $p > 0.05$). The water absorption was significantly higher for plain TPU

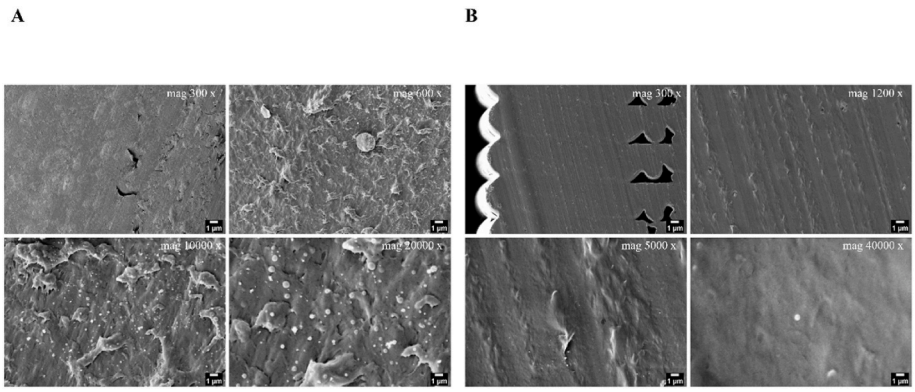

Fig. 6. Scanning electron microscope (SEM) images of (A) PLA-Cu and (B) TPU-Cu filament cross-section with increasing magnification.

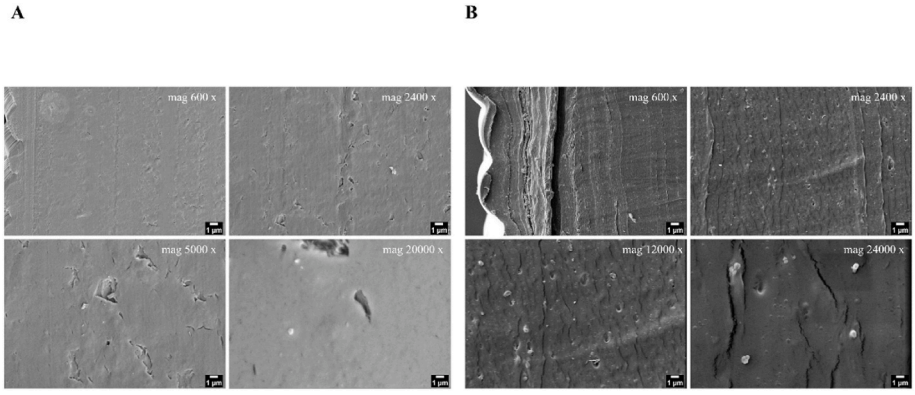

Fig. 7. Scanning electron microscope (SEM) images of (A) PLA-Ag and (B) TPU-Ag filament cross-section with increasing magnification.

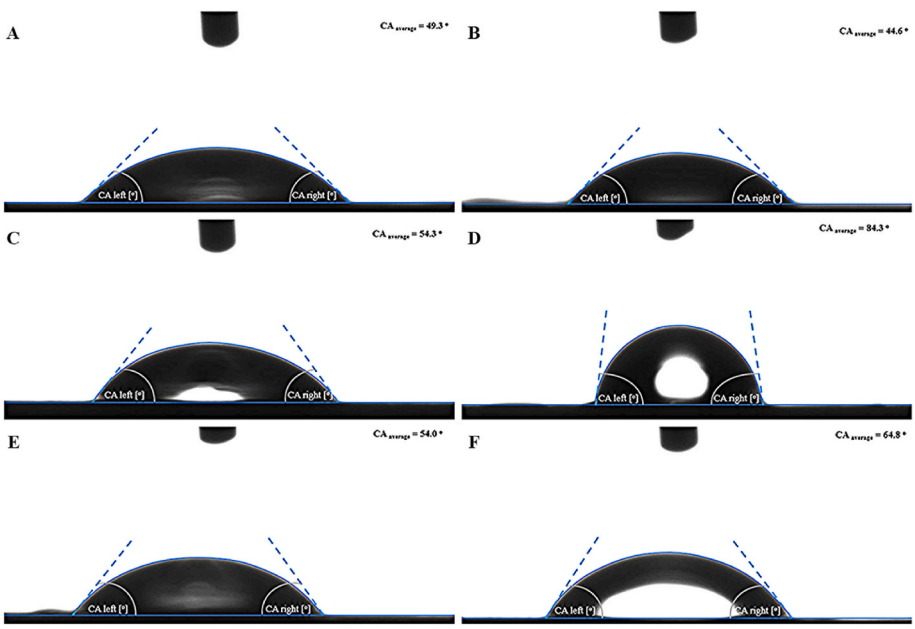

Fig. 8. Contact angle profiles of (A) plain PLA, (B) plain TPU, (C) PLA-Cu, (D) TPU-Cu, (E) PLA-Ag, and (F) TPU-Ag 3D printed surfaces at 0.10 mm layer height, revealing the hydrophobic properties and the wettability of the various 3D printed surfaces. The values presented are the mean of three droplets at three different locations ± SD.

(5.34 ± 1.64%), followed by TPU-Cu (5.08 ± 0.49%), whereas TPU-Ag (2.77 ± 0.26%) exhibited significantly lower water absorption capacity (Fig. 9; $p < 0.05$). The increased water absorption identified for the plain TPU and TPU-Cu surfaces can be attributed to the small porous and interlayer voids usually present when printing flexible materials like TPU. The lower water absorption of the 3D printed PLA surfaces loaded with Ag and Cu is probably due to the presence of the NPs and the physical characteristics of the PLA material, which is inflexible (Alam

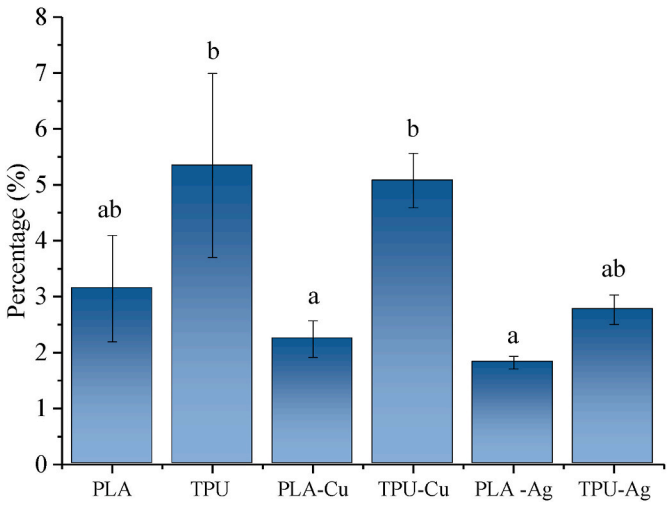

Fig. 9. Water absorption capacity of the different 3D printed surfaces after immersion in distilled water for 24 h at room temperature. Columns represent the mean values of 6 replicates ± SD. Different lowercase letters represent significant differences among different 3D printed surfaces ($p < 0.05$).

et al., 2020). In all cases, the water absorption capacity was lower than 6%, showing a high hydrophobicity of all surfaces, making PLA and TPU perfect candidates for their use in the fabrication of food and biomedical surfaces and equipment. Similarly, Ecker et al. (2019) observed that the 3D printed PLA specimens presented a 6% increase in water capacity that was further increased for PLA-wood 3D printed specimens due to the addition of 20% wood powder in the composite.

Moreover, the tensile properties that impact the strength and morphology of PLA and TPU filaments are directly connected with water absorption. Higher water content values result in more of these properties being affected and thus leading to lower quality of 3D printing.

3.4. Tensile behavior of PLA and TPU materials

Fig. 10 shows the stress-strain responses of PLA under quasi-static tensile loading. A general observation indicates that all three orientations present similar stress-strain curves for PLA, PLA-Cu, and PLA-Ag; both XY and XZ specimens ruptured approximately at 3% strain for all materials, whereas ZX specimen ruptured at 1% strain for PLA and PLA-Cu but 0.5% strain for PLA-Ag, respectively. The relatively lower stress-strain values of specimens built along the Z-axis reflect the bonding strength between successive layers in FDM process, which is influenced mainly by the choice of layer thickness and other inter-related processing parameters (Arif et al., 2018). The average stiffness values for the three orientations of PLA, PLA-Cu, and PLA-Ag are found to be (E_{PLA} = 1.89 GPa, $E_{PLA\text{-}Cu}$ = 1.99 GPa & $E_{PLA\text{-}Ag}$ = 2.12 GPa), indicating that Cu and Ag loaded material shows marginally stiffer response than plain PLA. This unique similarity of the stiffness across three orientations means that the described Young's modulus values can be respectively used in the design calculation or in the Finite Element Analysis assuming isotropic and linear materials with the known strain limits.

Fig. 11, illustrates the stress-strain responses of TPU, and the corresponding data is extracted to the strain limit of 100%, at which point the ZX specimens ruptured but all other specimens are observed to fail at much greater strain values (the graph shows the strain limit up to 1 for clarity and ease of comparison across different cases). It is noted that the family of TPU curves exhibits similar trends for all three orientations, but the differences in the Shore A hardness values (Table 1: 92A for TPU, 98A for TPU-Cu, and 90A for TPU-Ag) across all three materials make it unrealistic for a direct comparison between loaded and plain materials. When a comparison across three orientations of the same materials is made, XZ presents slightly lower stiffness than XY and ZX; this variation reflects the fact that long and slender tensile specimens are difficult to manufacture to achieve consistent wall thickness, especially in XZ and ZX orientations due to its softness and support structure requirement. The wrinkling issue (Fig. 3B) and the void formation (Figs. 5B and 6B) during the print, evidenced by the SEM analysis, contributed to the overall quality of the tensile specimens. TPU materials, which are non-linear in nature with high elongation at break, can be typically characterized as hyperelastic material models, as demonstrated in the prior studies (Adams et al., 2019; Robinson et al., 2019). For the comparative purpose, however, the linear portion of the curves (i.e., <10% strain) can be translated into Young's modulus values of (E_{TPU} = 59 MPa), ($E_{TPU\text{-}Cu}$ = 52 MPa) and ($E_{TPU\text{-}Ag}$ = 20 MPa), respectively.

3.5. In vitro antimicrobial effect of 3D printed surfaces against biofilm formation

The ability of various pathogenic bacteria to attach to hospital and food processing surfaces and equipment to form biofilms in inaccessible to clean locations has become of paramount importance for the food industry and healthcare facilities. Therefore, new techniques need to be adopted to enable better control against the most common pathogens causing these problems and ensure safety. The current study investigates the biofilm formation by *S. aureus* NCTC 12981, *S.* Typhimurium ATCC 14028, *E.coli* ATCC 25922, and *L. monocytogenes* NCTC 11994 on the surface of novel antimicrobial 3D printed surfaces loaded with Cu (Fig. 12) and Ag-NPs (Fig. 13). This is a novel approach to control the

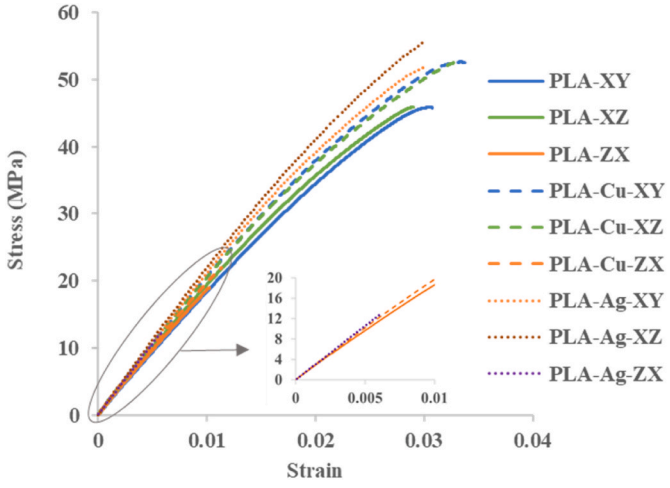

Fig. 10. Stress-strain curves of PLA, PLA-Cu, and PLA-Ag.

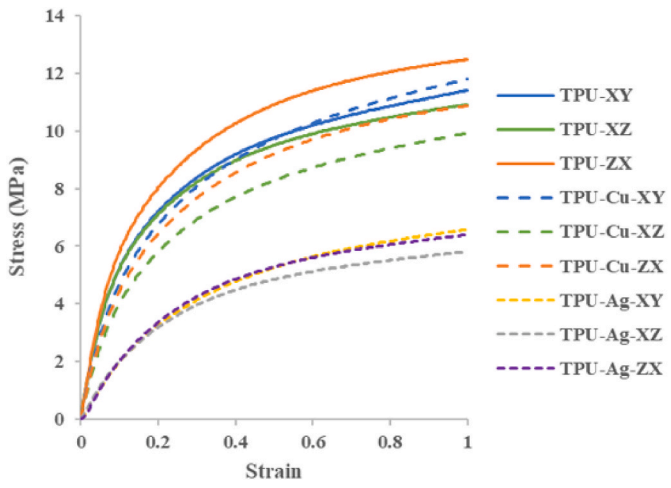

Fig. 11. Stress-strain curves of TPU, TPU-Cu, and TPU-Ag.

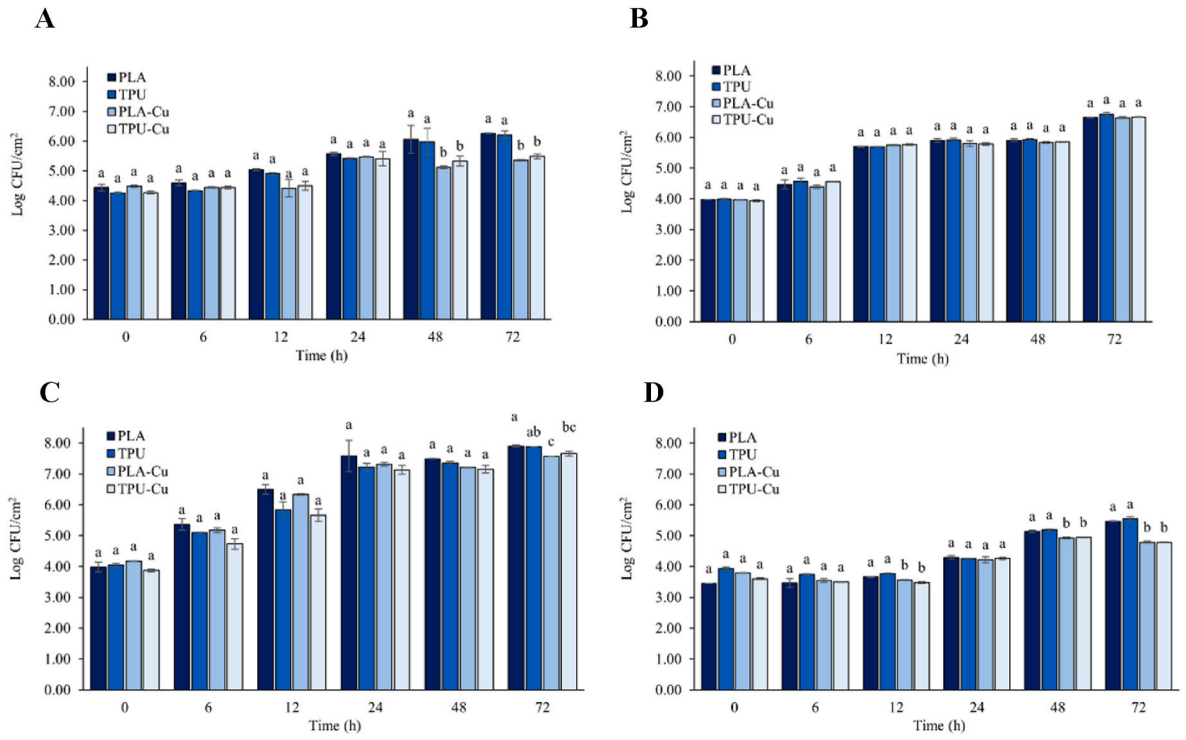

Fig. 12. The antimicrobial effect of the 3D printed surfaces fabricated using PLA and TPU filaments with or without Cu on biofilm formation of (A) *S. aureus* NCTC 12981, (B) *S*. Typhimurium ATCC 14028, (C) *E.coli* ATCC 25922, and (D) *L. monocytogenes* NCTC 11994 in TSB after 0, 6, 12, 24, 48, and 72 h. Columns represent the mean values of three independent experiments with two technical replicates. The error bars represent the mean's standard deviation (n = 6). Different lowercase letters represent significant differences among different time points ($p < 0.05$).

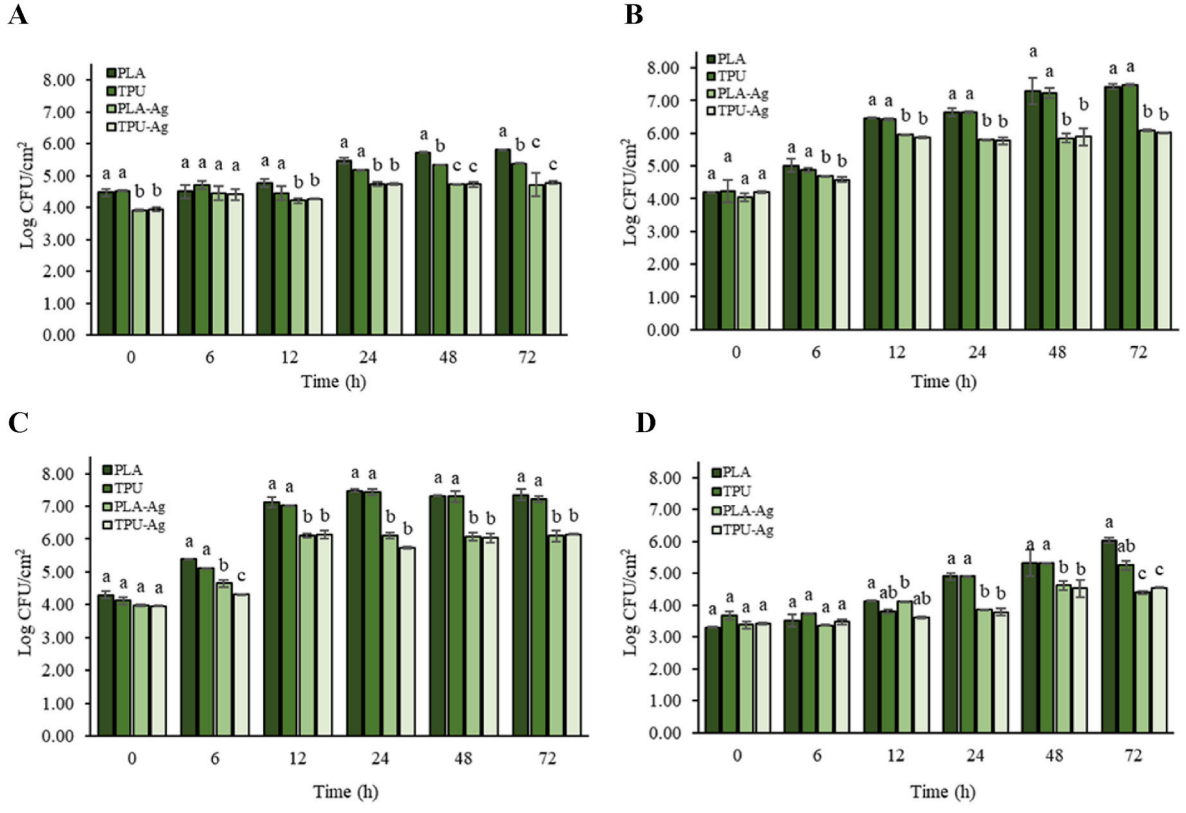

Fig. 13. The antimicrobial effect of the 3D printed surfaces fabricated using PLA and TPU filaments with or without Ag on biofilm formation of (A) *S. aureus* NCTC 12981, (B) *S*. Typhimurium ATCC 14028, (C) *E.coli* ATCC 25922, and (D) *L. monocytogenes* NCTC 11994 in TSB after 0, 6, 12, 24, 48, and 72 h. Columns represent the mean values of three independent experiments with two technical replicates. The error bars represent the mean's standard deviation (n = 6). Different lowercase letters represent significant differences among different time points ($p < 0.05$).

biofilm growth from healthcare and food contact surfaces.

The initial population of *S. aureus*, *S.* Typhimurium, *E.coli*, and *L. monocytogenes* on plain PLA was 4.43, 3.98, 3.98, and 3.45 Log CFU/cm^2 and on plain TPU 3D printed surfaces was 4.26, 3.98, 4.05, and 3.93, respectively (Fig. 12A, B, C, D). After 24 h, no statistically significant antimicrobial effect was observed on the biofilm growth of all four pathogens among the 3D printed surfaces with or without Cu addition. At the same time, *S. aureus* (Fig. 12A) and *L. monocytogenes* (Fig. 12D) were increased by more than 1-Log CFU/cm^2 and *S.* Typhimurium (Fig. 12B) and *E. coli* (Fig. 12C) revealed a more rapid increase by more than 2.5-Log CFU/cm^2. Interestingly, after 48 and 72 h, an inhibitory effect of the PLA-Cu and TPU-Cu 3D printed surfaces was observed on the mature biofilm cells of *S. aureus* and *L. monocytogenes*. The final levels of *S. aureus* on PLA-Cu (5.35 Log CFU/cm^2) and TPU-Cu (5.48 Log CFU/cm^2) surfaces after 72 h were significantly lower compared with the 6.26 and 6.21 Log CFU/cm^2 on plain PLA and TPU surfaces, respectively (Fig. 12A; $p < 0.05$). These observations agree with the results Kiel et al. (2022) reported that the biofilm-forming potential of *S. aureus* on plain PLA and the same commercial PLA loaded with Cu-NPs. The authors noticed the attachment of *S. aureus* biofilm cells on plain PLA and PLA-Cu after 24 h and approximately 1-Log reduction at adhered biofilm cells of *S. aureus* ATCC 25923 indicating the antimicrobial effect of PLA-Cu. The authors concluded that PLA-Cu was effective only against the Gram-positive *S. aureus* ATCC 25923, while no effect was exhibited against the tested Gram-negative *E. coli* C and *P. aeruginosa* PA01. These results could explain the inhibitory effect of the PLA-Cu and TPU-Cu surfaces presented against *L. monocytogenes* in the current study. The inhibitory properties of Cu-loaded PLA and TPU surfaces are due to the antimicrobial nature of the Cu nanostructures derived from metals and metal oxides and are mainly caused by their direct contact with the microorganisms (Makvandi et al., 2020). The exact antibacterial mechanism of action of the Cu-NPs remains unclear, while some hypothetical scenarios have been proposed. The first proposed mechanism describes the disruption of the bacterial membrane due to the CU-NPs' aggregation on the bacterial cell surface (Stankic et al., 2016). Subsequently, it is caused leakage of the intracellular components, and the Cu-NPs penetrate into the cell (Ahmed et al., 2021). It has also been described that Cu-NPs can release metal ions that can lead to the acceleration of reactive species (ROS) and hydroxyl radicals (HO•) production and lethally damage the cell's DNA and denature the proteins (Pramanik et al., 2012).

Ag-NPs are favored over NPs prepared from other metal alloys, as it has been shown that Ag is more antibacterial toward a wide range of bacterial species (Makvandi et al., 2020). To evidence the above scenario, the antimicrobial effect of PLA-Ag and TPU-Ag 3D printed surfaces was tested against the same four pathogens, and the results are presented in Fig. 12. The initial population of *S. aureus* on PLA-Ag and on TPU-Ag 3D printed surfaces were 3.91 and 3.94 Log CFU/cm^2 and significantly lower compared to the plain PLA (4.47 Log CFU/cm^2) and plain TPU (4.52 Log CFU/cm^2) surfaces (Fig. 12A; $p < 0.05$). In addition, no significant difference in the initial population of *S.* Typhimurium, *E. coli*, and *L. monocytogenes* biofilm cells on PLA-Ag and TPU-Ag 3D printed surfaces was observed compared with the plain PLA and TPU (Fig. 12B,C, and D; $p > 0.05$). After 12 h, a robust inhibitory effect was pronounced for the biofilm cells of *S. aureus*, *S.* Typhimurium, *E.coli*, and *L. monocytogenes* on PLA-Ag and TPU-Ag 3D printed surfaces. Many works documented the antibacterial effect of 3D printed specimens loaded with Ag-NPs against both Gram-positive and Gram-negative pathogens (Alam et al., 2020; Podstawczyk et al., 2020; Vidakis et al., 2020). However, in the current study we investigated not only the antimicrobial but the inhibitory effect of Ag-loaded 3D printed PLA and TPU surfaces against the most resistant biofilm cells of different maturity of four common food and nosocomial pathogens. The highest inhibitory effect was observed against *S.* Typhimurium. The bacterial growth was suppressed and remained close to 6-log CFU/cm^2 for the mature biofilm cells (72 h) on PLA-Ag and TPU-Ag surfaces, while the final population after 72 h on plain PLA and TPU was significantly higher and equal to 7.42 and 7.48 Log CFU/cm^2, respectively (Fig. 13B; $p < 0.05$). Moreover, the differences in the final cell population after 72 h among plain PLA and TPU surfaces and the surfaces loaded with Ag-NPs were statistically significant and ranged from 0.6 to 1-Log for *S. aureus* (Fig. 13A; $p < 0.05$) up to more than 1-Log CFU/cm^2 for *E. coli*, and *L. monocytogenes* (Fig. 13C and D; $p < 0.05$). Hall et al. (2021) explored the biofilm-forming ability of *E. coli* C, *P. aeruginosa* PA01, and *S. aureus* ATCC 29923 during 24 h growth on PLA 3D printed specimens loaded with various potentially antibacterial metal alloys including Ag and Cu. In the case of *E. coli* C and *S. aureus* ATCC 29923, the results showed a slight delay in growth and lower final cell densities compared with the control, also they showed results revealed that the most effective polymer in terms of antimicrobial properties was the one loaded with 33–40% Brass metal powder. However, these results need to be seen with caution as this was a very high load that it is well known to create critical problems on the quality of the final 3D prints and their mechanical properties (González-Henríquez et al., 2019; Russias et al., 2006). Several metal ions/alloys have been incorporated to prepare antibacterial materials compatible with 3D printing technology, but their final printability needs to be optimized before their application. An explanation of this can be found in the work of Podstawczyk et al. (2020). The authors presented a method to produce antimicrobial PLA filament by incorporating Ag-NPs (0.01–5 wt%). It was exhibited that the antibacterial effect against *S aureus* ATCC 6538, *E. coli* ATCC 10536, and *P. aeruginosa* ATCC15442 increased with the greater content of Ag-NPs and discussed that $AgNO_3$ content in PLA above 2.5% w/w deteriorates the surface quality of 3D printed parts and serves as an upper limit.

In the current study, we used commercial antibacterial filaments loaded with Ag-NPs, which displayed a higher inhibitory effect against Gram-positive *S. aureus* and *L. monocytogenes* than the Gram-negative *S.* Typhimurium and *E. coli*. Vidakis et al. (2020) observed the same effect with a higher Ag-NP susceptibility of Gram-negative bacteria over the Gram-positive ones. A higher sensitivity of Gram-negative bacteria over Gram-positive bacteria can be explained by the differences in the concentration of peptidoglycan in the cell wall. The Ag-NPs can adhere to the surface of the bacteria and alter their membrane properties. After entering the bacterial cell, the Ag-NPs can result in DNA damage. Another important mechanism of the antimicrobial activity of the Ag-NPs relies on their dialysis, which releases antimicrobial silver ions. The released silver ions interact with thiol-containing proteins in the cell wall and finally affect their functions (Durán et al., 2016).

The antimicrobial effect of 3D printed parts against numerous pathogens using filaments loaded with titanium (Palka et al., 2020), Graphene (Angulo-Pineda et al., 2020), Zinc (Ahmed et al., 2021), Brass (Hall et al., 2021), Aluminum (Hall et al., 2021) alloys and other antimicrobial compounds (Ahmed et al., 2018; Burgos et al., 2017; Sandler et al., 2014) have been studied showing the potential towards the broader adoption of 3D printed equipment and surfaces to prevent the growth of resistant biofilm cells and increase the overall microbiological safety in the food and healthcare sector.

3.6. Transferability of biofilm cells from 3D printed surfaces

Direct transferability is a newly introduced standard method that can be used to investigate the routine practice of disinfectants to decontaminate high-touch environmental surfaces or test the transferability of bacteria from one surface to another (Ledwoch et al., 2021; Sattar et al., 2015). This is the first study investigating the direct transferability of pathogenic biofilm cells with different maturity from the 3D printed surfaces with or without Cu or Ag (Table S1, Appendix).

Overall, all the tested 3D printed surfaces were ineffective in reducing the bacterial transferability of *S. aureus*, *S.* Typhimurium, *E. coli*, and *L. monocytogenes*. There was no difference among the different 3D printed surfaces, pathogens, or biofilms' maturity levels. However, in

some cases, a decrease in the number of positive contacts for bacterial growth was observed, such as for *L. monocytogenes* mature biofilm cells (72 h) that grew on PLA and TPU loaded with Cu or Ag-NPs but failed to prevent direct bacterial transfer. The current study can provide helpful information for the bacterial survival of some of the most common pathogens colonizing and forming resistant biofilms on 3D printed surfaces with or without antibacterial effects. However, further work is needed to investigate the effect on other bacterial pathogens and other types of 3D printable polymers to set practical and realistic guidelines for the food industry and health sector.

3.7. Proof of concept – sample print

Two examples of 3D printing using PLA-Ag and TPU-Cu filaments are presented in Figs. 14 and 15. The prosthetic leg socket shown in Fig. 14 is developed into a soft inner layer and hard outer layer from the scanned data. Both layers were printed together so that two materials permanently adhered to each other. The inner part was printed using TPU-Cu, and the outer surface was printed using PLA-Ag. This was designed to fit a child with a leg amputation, with the final dimensions being 55.16 x 64.28 x 87.09 mm^3. Children use the majority of 3D-printed prostheses due to their small size, constant growth, and psychosocial development (ten Kate et al., 2017). The prosthetic leg socket was printed using the Flashforge, Creator Pro 2 printer having two separate nozzles that were used to print two filaments at the same time without color mixing or technical failure on the final 3D printed prostheses. The prosthetic leg socket itself is made out of lightweight and durable materials and serves as the structural support. However, a prosthetic part can mainly get contaminated with *Staphylococcus* sp., forming biofilms and causing deformation of the prosthesis itself and severe health issues to the host (Bellón et al., 2001). From a design perspective, the mechanical data available from section 3.4 can be used to fine-tune the prosthetic's structure following BS EN ISO 10328-2016 (International Organization for Standardization, 2006).

In Fig. 15, a suggested door handle cover was printed using the flexible TPU-Cu. The final dimensions of the door handle cover were 19.76 x 19.75 x 71.00 mm^3 and it was printed vertically in 90^o without any additional supports. Door handles belong in the high-touch environmental surfaces, and not much attention has been given to bacterial biofilms colonizing these surfaces, despite their widespread presence on food and healthcare surfaces (Sattar et al., 2015). Appropriate decontamination with various disinfectants and disinfectant wipes can reduce the risk of contamination of the healthcare and food handlers and, subsequently, the food. However, multidrug-resistant (MDR) bacteria are becoming increasingly present in all settings and have been recognized by the World Health Organization (WHO) as a growing threat (Palmore and Henderson, 2013). In this context, new antimicrobial strategies, such as 3D printed antimicrobial surfaces, can be adopted to kill or inhibit the growth of MDR and persistent bacteria. In addition, 3D printing provides a promising possibility for individualization, personalized color, shape, and size without the need to adjust the production machine. Importantly, it should be taken under consideration that the addition of Cu or Ag could result in toxic effects on some occasions if they come in contact with human tissue. However, studies have shown the incorporation of Cu and Ag in low concentrations poses no or very low risk of adverse skin reactions or after digestion (Böhmert et al., 2014; Hostynek and Maibach, 2004; Jaswal and Gupta, 2021). However, future work should include toxicity studies to prove the safety of the antibacterial composites before their adoption.

4. Conclusions

Cu and Ag and their alloys are a type of metallic biomaterials that have been increasingly used in many medical devices, and due to their biocompatibility, mechanical and anticorrosive properties are being used in the food sector. The current study's advantages lie in the optimization process to print compact 3D surfaces with increased accuracy and enhanced mechanical and antimicrobial properties against Gram-positive and Gram-negative pathogens to tackle the problem of biofilm colonization on food and healthcare surfaces. We have shown that the 3D printed surfaces loaded with Cu and Ag-NPs inhibited the biofilm formation of the most common foodborne and nosocomial pathogens. Among all samples, PLA-Ag and TPU-Ag 3D printed surfaces revealed excellent mechanical properties and inhibitory efficacy. Additionally, the use of these antimicrobial polymers to print prosthetic parts and high-touch surfaces such as door handles presented in the current study are only some of the numerous applications this technology can offer to reduce the risk of bacterial contamination and biofilm formation.

The approach of using 3D printing for applications in the food industry and healthcare sectors is relatively new but very promising. Our results provide new insights on manufacturing antibacterial food and medical surfaces and equipment with promising mechanical and antimicrobial properties.

Funding

This research was funded by an internal competitive grant awarded to Alexandros Ch. Stratakos and Shwe Soe from the University of the West of England, Bristol.

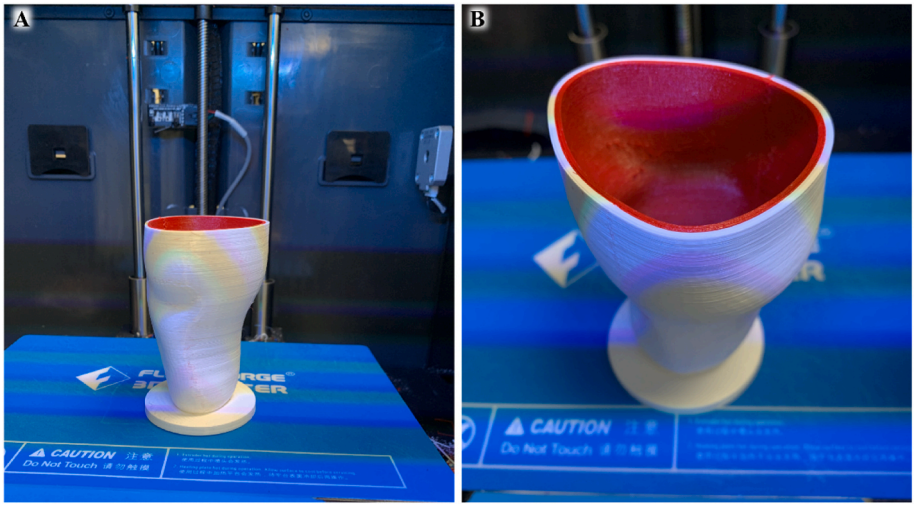

Fig. 14. The original sample of 3D printed prosthetic leg from a (A) distant and (B) close-up view.

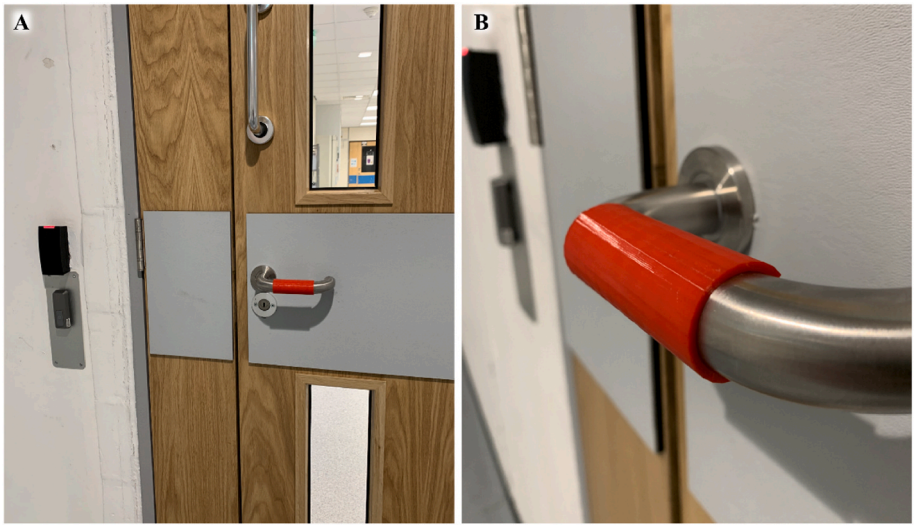

Fig. 15. The original sample of 3D printed door handle socket from a (A) distant and (B) close-up view.

CRediT authorship contribution statement

Sotirios I. Ekonomou: Writing – original draft, Validation, Software, Methodology, Investigation, Formal analysis, Data curation. **Shwe Soe:** Supervision, Resources, Funding acquisition, Writing - review & editing. **Alexandros Ch Stratakos:** Writing – review & editing, Supervision, Resources, Funding acquisition, Conceptualization.

Declaration of competing interest

The authors declare that they have no known competing financial interests or personal relationships that could have appeared to influence the work reported in this paper.

Data availability

Data will be made available on request.

Acknowledgments

The authors would like to thank Dr. David Patton for his valuable assistance with SEM analysis and Tamsila Tauqir for assisting with tensile testing.

Appendix A. Supplementary data

Supplementary data to this article can be found online at https://doi.org/10.1016/j.jmbbm.2022.105536.

References

Adams, R., Soe, S.P., Santiago, R., Robinson, M., Hanna, B., McShane, G., Alves, M., Burek, R., Theobald, P., 2019. A novel pathway for efficient characterisation of additively manufactured thermoplastic elastomers. Mater. Des. 180, 107917 https://doi.org/10.1016/j.matdes.2019.107917.

Ahmed, J., Arfat, Y.A., Bher, A., Mulla, M., Jacob, H., Auras, R., 2018. Active chicken meat packaging based on polylactide films and bimetallic Ag-Cu nanoparticles and essential oil. J. Food Sci. 83, 1299–1310. https://doi.org/10.1111/1750-3841.14121.

Ahmed, W., Siraj, S., Al-Marzouqi, A.H., 2021. Embracing additive manufacturing technology through fused filament fabrication for antimicrobial with enhanced formulated materials. Polymers 13. https://doi.org/10.3390/polym13091523.

Alam, F., Shukla, V.R., Varadarajan, K.M., Kumar, S., 2020. Microarchitected 3D printed polylactic acid (PLA) nanocomposite scaffolds for biomedical applications. J. Mech. Behav. Biomed. Mater. 103, 103576 https://doi.org/10.1016/j.jmbbm.2019.103576.

Aliheidari, N., Tripuraneni, R., Ameli, A., Nadimpalli, S., 2017. Fracture resistance measurement of fused deposition modeling 3D printed polymers. Polym. Test. 60, 94–101. https://doi.org/10.1016/j.polymertesting.2017.03.016.

Angulo-Pineda, C., Srirussamee, K., Palma, P., Fuenzalida, V.M., Cartmell, S.H., Palza, H., 2020. Electroactive 3D printed scaffolds based on percolated composites of polycaprolactone with thermally reduced graphene oxide for antibacterial and tissue engineering applications. Nanomaterials 10, 428. https://doi.org/10.3390/nano10030428.

Arif, M.F., Kumar, S., Varadarajan, K.M., Cantwell, W.J., 2018. Performance of biocompatible PEEK processed by fused deposition additive manufacturing. Mater. Des. 146, 249–259. https://doi.org/10.1016/j.matdes.2018.03.015.

Ashrafudoulla, M., Rahaman Mizan, M.F., Park, S.H., Ha, S. Do, 2021. Antibiofilm activity of carvacrol against Listeria monocytogenes and Pseudomonas aeruginosa biofilm on MBEC^{TM} biofilm device and polypropylene surface. Lebensm. Wiss. Technol. 147, 111575 https://doi.org/10.1016/j.lwt.2021.111575.

Astm, D., 2010. ASTM D570-98 Standard Test Method for Water Absorption of Plastics. ASTM Int., West Conshohocken Pennsylvania.

BS ISO 37, 2011. BS ISO 37:2011 - rubber, vulcanized or thermoplastic - determination of tensile stress-strain properties. International Standard.

Ban, G.H., Kang, D.H., 2016. Effect of sanitizer combined with steam heating on the inactivation of foodborne pathogens in a biofilm on stainless steel. Food Microbiol. 55, 47–54. https://doi.org/10.1016/j.fm.2015.11.003.

Bellón, J.M., G-Honduvilla, N., Jurado, F., G-Carranza, A., Buján, J., 2001. In vitro interaction of bacteria with polypropylene/ePTFE prostheses. Biomaterials 22, 2021–2024. https://doi.org/10.1016/S0142-9612(00)00390-2.

Bintsis, T., 2017. Foodborne pathogens. AIMS Microbiol 3, 529–563. https://doi.org/10.3934/microbiol.2017.3.529.

Böhmert, L., Girod, M., Hansen, U., Maul, R., Knappe, P., Niemann, B., Weidner, S.M., Thünemann, A.F., Lampen, A., 2014. Analytically monitored digestion of silver nanoparticles and their toxicity on human intestinal cells. Nanotoxicology 8, 631–642. https://doi.org/10.3109/17435390.2013.815284/SUPPL_FILE/INAN_A_815284_SM0001.DOC.

Burgos, N., Armentano, I., Fortunati, E., Dominici, F., Luzi, F., Fiori, S., Cristofaro, F., Visai, L., Jiménez, A., Kenny, J.M., 2017. Functional properties of plasticized bio-based poly(lactic Acid)_Poly(hydroxybutyrate) (PLA_PHB) films for active food packaging. Food Bioprocess Technol. 10, 770–780. https://doi.org/10.1007/s11947-016-1846-3.

Cao, Q., Cai, Y., Jing, B., Liu, P., 2006. Structure and mechanical properties of thermoplastic polyurethane, based on hyperbranched polyesters. J. Appl. Polym. Sci. 102, 5266–5273. https://doi.org/10.1002/app.24779.

Carpentier, B., Cerf, O., 2011. Review - persistence of Listeria monocytogenes in food industry equipment and premises. Int. J. Food Microbiol. 145, 1–8. https://doi.org/10.1016/j.ijfoodmicro.2011.01.005.

Choonara, Y.E., Du Toit, L.C., Kumar, P., Kondiah, P.P.D., Pillay, V., 2016. 3D-printing and the effect on medical costs: a new era? Expert Rev. Pharmacoecon. Outcomes Res. 16, 23–32. https://doi.org/10.1586/14737167.2016.1138860.

Deb, D., Jafferson, J.M., 2021. Natural fibers reinforced FDM 3D printing filaments. In: Materials Today: Proceedings. Elsevier, pp. 1308–1318. https://doi.org/10.1016/j.matpr.2021.02.397.

Durán, N., Durán, M., de Jesus, M.B., Seabra, A.B., Fávaro, W.J., Nakazato, G., 2016. Silver nanoparticles: a new view on mechanistic aspects on antimicrobial activity. Nanomed. Nanotechnol. Biol. Med. 12, 789–799. https://doi.org/10.1016/j.nano.2015.11.016.

Ecker, J.V., Haider, A., Burzic, I., Huber, A., Eder, G., Hild, S., 2019. Mechanical properties and water absorption behaviour of PLA and PLA/wood composites prepared by 3D printing and injection moulding. Rapid Prototyp. J. 25, 672–678. https://doi.org/10.1108/RPJ-06-2018-0149.

González-Henríquez, C.M., Sarabia-Vallejos, M.A., Hernandez, J.R., 2019. Antimicrobial polymers for additive manufacturing. Int. J. Mol. Sci. 20 https://doi.org/10.3390/ijms20051210.

Hall, D.C., Palmer, P., Ji, H.F., Ehrlich, G.D., Król, J.E., 2021. Bacterial biofilm growth on 3D-printed materials. Front. Microbiol. 12, 1–13. https://doi.org/10.3389/fmicb.2021.646303.

Hostynek, J.J., Maibach, H.I., 2004. Copper hypersensitivity: dermatologic aspects. Dermatol. Ther. 17, 328–333. https://doi.org/10.1111/J.1396-0296.2004.04035.X.

Hutmacher, D.W., Schantz, T., Zein, I., Ng, K.W., Teoh, S.H., Tan, K.C., 2001. Mechanical properties and cell cultural response of polycaprolactone scaffolds designed and fabricated via fused deposition modeling. J. Biomed. Mater. Res. 55, 203–216. https://doi.org/10.1002/1097-4636, 200105)55:2<203::aid-jbm1007>3.3.co;2-z.

International Organization for Standardization, 2006. Prosthetics – Structural Testing of Lower Limb Prostheses. ISO 10328, 61010-1 © Iec:2001.

ISO-International Organization for Standardization, 2012. EN ISO 527-1 & 4-1993 Determination of Tensile Properties_general Principles. Geneva.

Jašo, V., Glenn, G., Klamczynski, A., Petrović, Z.S., 2015. Biodegradability study of polylactic acid/thermoplastic polyurethane blends. Polym. Test. 47, 1–3. https://doi.org/10.1016/j.polymertesting.2015.07.011.

Jaswal, T., Gupta, J., 2021. A review on the toxicity of silver nanoparticles on human health. Mater. Today Proc. https://doi.org/10.1016/j.matpr.2021.04.266.

Kenawy, E.R., Worley, S.D., Broughton, R., 2007. The chemistry and applications of antimicrobial polymers: a state-of-the-art review. Biomacromolecules 8, 1359–1384. https://doi.org/10.1021/BM061150Q/ASSET/IMAGES/LARGE/BM061150QF00031. JPEG.

Kiel, A., Kaltschmidt, B.P., Asghari, E., Hütten, A., Kaltschmidt, B., Kaltschmidt, C., 2022. Bacterial biofilm formation on nano-copper added PLA suited for 3D printed face masks. Microorganisms 10. https://doi.org/10.3390/microorganisms10020439.

Ledwoch, K., Dancer, S.J., Otter, J.A., Kerr, K., Roposte, D., Rushton, L., Weiser, R., Mahenthiralingam, E., Muir, D.D., Maillard, J.Y., 2018. Beware biofilm! Dry biofilms containing bacterial pathogens on multiple healthcare surfaces; a multi-centre study. J. Hosp. Infect. 100, e47–e56. https://doi.org/10.1016/J.JHIN.2018.06.028.

Ledwoch, K., Said, J., Norville, P., Maillard, J.Y., 2019. Artificial dry surface biofilm models for testing the efficacy of cleaning and disinfection. Lett. Appl. Microbiol. 68, 329–336. https://doi.org/10.1111/lam.13143.

Ledwoch, K., Magoga, M., Williams, D., Fabbri, S., Walsh, J., Maillard, J.Y., 2021. Is a reduction in viability enough to determine biofilm susceptibility to a biocide? Infect. Control Hosp. Epidemiol. 42, 1486–1492. https://doi.org/10.1017/ice.2021.42.

Lee, S.H., Jun, B.H., 2019. Silver nanoparticles: synthesis and application for nanomedicine. Int. J. Mol. Sci. 20 https://doi.org/10.3390/ijms20040865.

Lineback, C.B., Nkemngong, C.A., Wu, S.T., Li, X., Teska, P.J., Oliver, H.F., 2018. Hydrogen peroxide and sodium hypochlorite disinfectants are more effective against Staphylococcus aureus and Pseudomonas aeruginosa biofilms than quaternary ammonium compounds. Antimicrob. Resist. Infect. Control 7, 1–7. https://doi.org/10.1186/S13756-018-0447-5/FIGURES/2.

Mai, H.N., Hyun, D.C., Park, J.H., Kim, D.Y., Lee, S.M., Lee, D.H., 2020. Antibacterial drug-release polydimethylsiloxane coating for 3d-printing dental polymer: surface alterations and antimicrobial effects. Pharmaceuticals 13, 1–12. https://doi.org/10.3390/ph13100304.

Makvandi, P., Gu, J.T., Zare, E.N., Ashtari, B., Moeini, A., Tay, F.R., Niu, L. na, 2020. Polymeric and inorganic nanoscopical antimicrobial fillers in dentistry. Acta Biomater. 101, 69–101. https://doi.org/10.1016/j.actbio.2019.09.025.

Muwaffak, Z., Goyanes, A., Clark, V., Basit, A.W., Hilton, S.T., Gaisford, S., 2017. Patient-specific 3D scanned and 3D printed antimicrobial polycaprolactone wound dressings. Int. J. Pharm. 527, 161–170. https://doi.org/10.1016/j.ijpharm.2017.04.077.

Ngo, T.D., Kashani, A., Imbalzano, G., Nguyen, K.T.Q., Hui, D., 2018. Additive manufacturing (3D printing): a review of materials, methods, applications and challenges. Compos. B Eng. https://doi.org/10.1016/j.compositesb.2018.02.012.

Palka, L., Mazurek-Popczyk, J., Arkusz, K., Baldy-Chudzik, K., 2020. Susceptibility to biofilm formation on 3D-printed titanium fixation plates used in the mandible: a preliminary study. J. Oral Microbiol. 12, 1–11. https://doi.org/10.1080/20002297.2020.1838164.

Palmore, T.N., Henderson, D.K., 2013. Managing transmission of carbapenem-resistant enterobacteriaceae in healthcare settings: a view from the trenches. Clin. Infect. Dis. 57, 1593–1599. https://doi.org/10.1093/CID/CIT531.

Podstawczyk, D., Skrzypczak, D., Połomska, X., Stargała, A., Witek-Krowiak, A., Guiseppi-Elie, A., Galewski, Z., 2020. Preparation of antimicrobial 3D printing filament: in situ thermal formation of silver nanoparticles during the material extrusion. Polym. Compos. 41, 4692–4705. https://doi.org/10.1002/pc.25743.

Pramanik, A., Laha, D., Bhattacharya, D., Pramanik, P., Karmakar, P., 2012. A novel study of antibacterial activity of copper iodide nanoparticle mediated by DNA and membrane damage. Colloids Surf. B Biointerfaces 96, 50–55. https://doi.org/10.1016/J.COLSURFB.2012.03.021.

Quino, G., Tagarielli, V.L., Petrinic, N., 2020. Effects of water absorption on the mechanical properties of GFRPs. Compos. Sci. Technol. 199, 108316 https://doi.org/10.1016/j.compscitech.2020.108316.

Robinson, M., Soe, S., Johnston, R., Adams, R., Hanna, B., Burek, R., McShane, G., Celeghini, R., Alves, M., Theobald, P., 2019. Mechanical characterisation of additively manufactured elastomeric structures for variable strain rate applications. Addit. Manuf. 27, 398–407. https://doi.org/10.1016/j.addma.2019.03.022.

Russias, J., Saiz, E., Nalla, R.K., Gryn, K., Ritchie, R.O., Tomsia, A.P., 2006. Fabrication and mechanical properties of PLA/HA composites: a study of in vitro degradation. Mater. Sci. Eng. C 26, 1289–1295. https://doi.org/10.1016/j.msec.2005.08.004.

Sandler, N., Salmela, I., Fallarero, A., Rosling, A., Khajeheian, M., Kolakovic, R., Genina, N., Nyman, J., Vuorela, P., 2014. Towards fabrication of 3D printed medical devices to prevent biofilm formation. Int. J. Pharm. 459, 62–64. https://doi.org/10.1016/j.ijpharm.2013.11.001.

Sattar, S.A., Bradley, C., Kibbee, R., Wesgate, R., Wilkinson, M.A.C., Sharpe, T., Maillard, J.Y., 2015. Disinfectant wipes are appropriate to control microbial bioburden from surfaces: use of a new ASTM standard test protocol to demonstrate efficacy. J. Hosp. Infect. 91, 319–325. https://doi.org/10.1016/j.jhin.2015.08.026.

2012 Siedenbiedel, F., Tiller, J.C., 2012. Antimicrobial polymers in solution and on surfaces: overview and functional principles, 4 Polymer 4, 46–71. https://doi.org/10.3390/POLYM4010046, 46-71.

Stankic, S., Suman, S., Haque, F., Vidic, J., 2016. Pure and multi metal oxide nanoparticles: synthesis, antibacterial and cytotoxic properties. J. Nanobiotechnol. 141 (14), 1–20. https://doi.org/10.1186/S12951-016-0225-6, 2016.

Technical Committee AMT/8, 2017. BS EN ISO/ASTM 52900: additive manufacturing - general principles - terminology. Int. Stand. 1–30.

ten Kate, J., Smit, G., Breedveld, P., 2017. 3D-printed Upper Limb Prostheses: a Review. https://doi.org/10.1080/17483107.2016.1253117, 10.1080/17483107.2016.1253117 12, 300–314.

Vidakis, N., Petousis, M., Velidakis, E., Liebscher, M., Tzounis, L., 2020. Three-dimensional printed antimicrobial objects of polylactic acid (PLA)-Silver nanoparticle nanocomposite filaments produced by an in-situ reduction reactive melt mixing process. Biomimetics 5, 42. https://doi.org/10.3390/biomimetics5030042.